THE JOURNAL OF PHYSICAL CHEMISTRY C

Article

Cite This: J. Phys. Chem. C 2018, 122, 16664−16673

pubs.acs.org/JPCC

Reaction Stoichiometry and Mechanism of Pt Deposition via Surface Limited Redox Replacement of Copper UPD Layer on Au(111)

Qiuyi Yuan,[†] Yuki Wakisaka,[†] Yohei Uemura,[‡] Takahiro Wada,[§] Hiroko Ariga-Miwa,[†] Satoru Takakusagi,[†] Kiyotaka Asakura,*[,†] and Stanko R. Brankovic[∥]

[†]Intitute for Catalysis, Hokkaido University, Kita 21 Nishi 10, Kita-ku, Sapporo, Hokkaido 001-0021, Japan

[‡]Institute for Molecular Science, Okazaki, Aichi 444-0867, Japan

[§]Tokyo Medical and Dental University, 1-5-45, Yushima, Bunkyo-ku, Tokyo 113-8549, Japan

[∥]Department of Electrical and Computer Engineering, University of Houston, Houston, Texas 77204-4005, United States

Supporting Information

ABSTRACT: The stoichiometry and reaction mechanism of Pt deposition via surface limited redox replacement (SLRR) of Cu underpotential-deposited (UPD) monolayer on Au(111) was studied using in situ polarization dependent total reflection fluorescence X-ray absorption fine structure (PTRF-XAFS), scanning tunneling microscopy (STM), X-ray photoelectron spectroscopy (XPS), and cyclic voltammetry (CV). We proposed that Pt deposition via SLRR of Cu UPD monolayer leads to formation/deposition of Pt-surface species mainly consisting of Pt(II) chloride with a square planar local structure [$PtCl_4$] parallel to the Au surface (60%) which has a strong interaction of the Pt complex with the Au substrate. The rest (40%) was one-monolayer Pt metal cluster. This result provides a new understanding into the mechanism and stoichiometry of the SLRR reaction, which has a wide application for synthesis of monolayer catalysts.

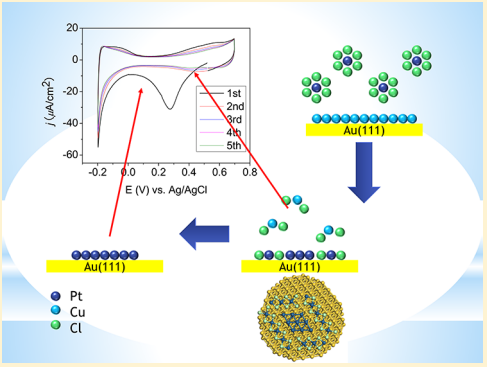

INTRODUCTION

Two-dimensional (2D) Pt thin films have been used in a variety of applications including microelectronics, energy conversion and storage, as well as biocompatible materials.[1,2] Among the different deposition methods such as molecular beam epitaxy (MBE),[3] chemical vapor deposition (CVD),[4] and physical vapor deposition (PVD),[5] the electrodeposition[6] as ambient temperature growth method offers certain advantages when simplicity and costs are considered. In particular, it is quite easy to control the amount and morphology of deposited metal films by varying the applied potential/current and time. In some substrate−metal ion systems, the phenomenon of underpotential deposition (UPD) provides a facile way to form monolayer/submonolayer epitaxial films by simple control of the electrode potential. However, in the case of noble metals such as Pt, the formation of the 2D film is quite difficult due to its high surface energy. Typically, a three-dimensional (3D) growth was observed.[7] However, in recent years, a new deposition method was developed based on the UPD monolayer serving as a reducing sacrificial template in the SLRR reaction (galvanic displacement) with more noble Pt ions.[8] The deposition protocol involves several steps in which the Au surface (substrate) is first covered with a UPD layer of Cu which plays a role as sacrificial metal and was displaced with Pt under open circuit potential (OCP). Since Pt is a material of pivotal importance as electrocatalyst for polymer electrolyte fuel cells (PEFCs),[9] this method has attracted a lot of attention, both, in the fundamental studies exploring for the deposition and SLRR reaction mechanism[10−13] and in practical studies to optimize the method[14,15] and to obtain the efficient electrocatalyst synthesis.[16,17] Weaver et al. first applied this method to grow Pt thin films repetitive SLRR reaction.[18] Later on, this approach was optimized by other groups to be developed as a standard electrodeposition method nowadays.[19] The studies of deposition via SLRR of the UPD monolayer has been expanded in several directions.[8,19−23] Recent development can be found in a review paper.[24] Although the modeling of the SLRR reaction kinetics has been discussed,[10,11,25,26] the insight into the atomic level structure of the deposited film and a molecular level understanding of the SLRR mechanism are still lacking. More experimental evidence is also necessary to fully understand the role of the substrate and other experimental parameters controlling the morphology of deposited films. In our previous study, in situ PTRF-XAFS (polarization dependent total reflection fluorescence-X-ray absorption fine structure) was applied in studying the Pt monolayer on Au(111) deposited via SLRR of Cu UPD layer.[27] PTRF-XAFS is extremely powerful in characterizing the structure and the electronic state of the submonolayer adsorption on an

Received: March 6, 2018
Revised: June 27, 2018
Published: July 2, 2018

DOI: 10.1021/acs.jpcc.8b02218
J. Phys. Chem. C 2018, 122, 16664−16673

atomically flat surface.[28−31] We found in PTRF-XAFS measurements that a Pt complex, [$PtCl_4$], absorbed on the Au surface was the main Pt species. This was an unexpected result, as fully reduced Pt had been expected as the main product. In order to understand the deposited film structure and the SLRR mechanism, we analyzed the XAFS data in combination with other characterization techniques including scanning tunneling microscopy (STM), X-ray photoelectron spectroscopy (XPS), and electrochemical methods. This approach allowed us the more detailed view about the SLRR reaction mechanism than the previous in situ XAFS report.[27] In this paper we propose the new structure of the Pt metal cluster surrounded by the [$PtCl_2$-square] species after the SLRR process. The SLRR mechanism is also discussed.

EXPERIMENTAL SECTION

Pt/Au(111) Sample Preparation and Electrochemical Characterization. The synthesis of Pt/Au(111) followed the galvanic displacement reaction protocol.[8] A ϕ = 10 mm Au(111) single crystal with 5 mm in thickness (purchased from SPL, The Netherlands) was used as the substrate. After the Au sample was electrochemically polished and flame-annealed, it was transferred to an Ar filled glovebox for further treatment. Figure S1a shows the cyclic voltammetry (CV) of Au(111). All chemicals were purchased from Alfa Aeser with ultrahigh grade (99.999%). 18.2 MΩ cm ultrapure water (UPW; Milli-Q, Merck Millipore Co) generated after UV photooxidation and nonporous filtering was used to make the solutions. All of the solutions were deareated with Ar for 1 h to minimize the oxygen content prior to the experiment. A three-electrode glass cell with Ag/AgCl as the reference electrode and a Pt coil as the counter electrode was used for Cu UPD. An HSV-110 potentiostat (Hokuto Denko) was used for all electrochemical measurements. Potentials were reported with respect to Ag/AgCl, unless otherwise denoted. The solution of 0.1 M $HClO_4$ + 1 mM $Cu(ClO_4)_2$ was used for Cu UPD. The UPD potential was determined by the CV scanned at the range from 0.42 to 0.03 V vs Cu/Cu^{2+} pseudoelectrode as shown in Figure S1b. The deposition potential was 0.03 V, where a full monolayer of Cu UPD was expected. After Cu UPD was formed, the sample was rinsed with UPW and dipped in the 0.1 M $HClO_4$ + 1 mM H_2PtCl_6 solution for 30 s to carry out the replacement reaction. We used Pt(IV) instead of Pt(II) just because Pt(IV) gives a Pt monolayer with more reproducibility and we would like to follow the original SLRR process.[10] The possible origin for less reproducibility of the Pt(II) species in the SLRR process was given later. The sample was rinsed again with UPW. Electrochemical characterization was also performed on the as-deposited surface by scanning CV in 0.1 M $HClO_4$.

XAFS Measurements and Analysis. To eliminate oxygen contamination, an in situ polychloro-trifluoroethylene (PCTFE) XAFS cell[27] was assembled in the glovebox. A Mylar film with thickness of 6 μm was used as the X-ray window. The solution thickness between the sample surface and Mylar film could be adjusted according to the preparation and measurement cases. In the preparation case the sample was retracted from the Mylar film with the distance around 1 cm to guarantee the thickness enough for the diffusion of the electrolyte to reach the sample surface smoothly. In the measurement case, the sample was placed near the Mylar film with the thickness of the solution on the order of tens of μm to minimize the X-ray absorbing and scattering of the solution during XAFS measurement. The counter electrode (CE) and reference electrode (RE) were both located in blanch glass containers attached to the cell body so that the electrodes in the containers could be shielded with Pb sheets to eliminate any contamination fluorescence from the electrodes. The assembled cell was filled with deaerated 0.1 M $HClO_4$ and was mounted on a 5-axis goniometer to adjust the polarization directions and total reflection conditions. We measured the Pt L_3 edge XAFS at BL12C in Photon Factory (2.5 GeV, 450 mA) of Institute of Materials Structure Science, High Energy Accelerator Research Organization (KEK-IMSS-PF). The monochromator was a Si(111) double crystal, and an X-ray beam was focused by the Rh coated cylindrical mirror. X-ray fluorescence was detected by a 19-element Ge solid state detector (MSSD; Canberra). To reduce the elastic scattering from both the solution layer and the Au substrate, a Zn filter (μt = 3) and a Soller slit were placed in front of the MSSD. We also carried out the PTRF-XAFS measurements in BL36XU in SPring-8 in the almost same experimental setup (proposal number of 2016B7904). The XAFS analysis including the background removal, Fourier transform, and curve fitting were carried out by REX2000.[32] Phase shift and amplitude functions were derived from FEFF8.[33,34] In our work, Pt L_3 edge EXAFS has the following polarization dependence:[35]

$$\chi^*(k, \Theta) = \frac{1}{2}\sum_{i=1}^{N}(1.2 + 2.4\cos^2\theta_i(\Theta))\chi_i(k) \quad (1)$$

where $\chi^*(k,\Theta)$ is total EXAFS oscillation while $\chi_i(k)$ is the EXAFS contribution from the ith bond. Θ is the angle between the electric field vector $\hat{e}$ and the surface normal vector. θ_i is the angle between the $\hat{e}$ and the ith bonding direction, r_i. The FEFF simulation was evaluated by

$$|R(\Theta)|^2 = \frac{1}{N_{data}}\sum_j \frac{(\chi^*_{data}(k_j, \Theta) - \chi^*_{fit}(k_j, \Theta))^2}{\varepsilon^2(k_j, \Theta)} \quad (2)$$

where N_{data} is the number of data points in fitting and $\chi^*_{data}(k_j,\Theta)$ and $\chi^*_{fit}(k_j,\Theta)$ are polarized experimental and fitted EXAFS data points, respectively. $\varepsilon(k_j,\Theta)$ is the standard deviation at each point.

XPS Measurements. To confirm chemical state and morphology, XPS and STM were done on the as-deposited sample directly after the galvanic displacement reaction.

XPS measurements were conducted with JPC-9010MC XPS (JEOL, Japan) under 1 × 10^{-6} Pa. The monochromatized Al Kα (1486.7 eV) was used to avoid the Au 4f peaks excited by X-ray satellite peaks. X-ray source current was set to 30 mA, while its voltage was set to 10 kV. The binding energies (BE) were calibrated by Au $4f_{7/2}$ set at 83.8 eV.[36] After the background removal using the Shirley method, Pt 4f spectra were fitted using Lorentzian−Gaussian curves to obtain BE and peak areas, fixing the doublet separation and peak area ratio.

STM Measurement. Ex situ STM of the as-deposited sample was done using Cypher AFM (Oxford Instrument). A freshly cut Pt−Ir (80:20) wire was used as the STM tip. The images were taken at the condition with a tunneling current of 0.8 nA and a bias voltage of 150 mV at the constant current mode. WSxM 5.0 was used for image analysis.[37] Coverage information was based on the analysis of more than 20 images.

DOI: 10.1021/acs.jpcc.8b02218
J. Phys. Chem. C 2018, 122, 16664−16673

RESULTS AND DISCUSSION

Electrochemical Results. Figure 1 shows the CV scans in 0.1 M $HClO_4$ of Pt/Au(111) after the SLRR of Cu UPD

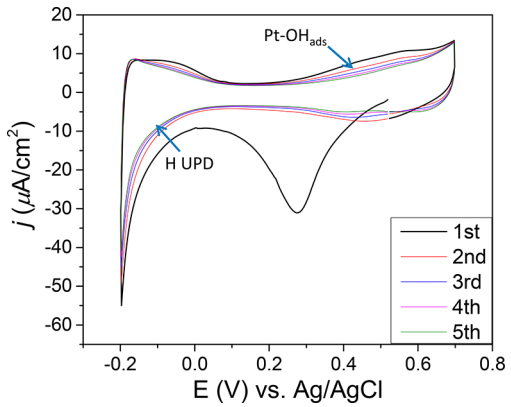

Figure 1. First five scans CV of Pt/Au(111) in 0.1 M $HClO_4$, starting from 0.5 V towards cathodic direction. Scan rate: 0.05 V/s.

monolayer using $[PtCl_6]^{2-}$ as the Pt precursor. A scan started from OCP at 0.5 V toward cathodic direction with the range from −0.2 to +0.7 V. Basically, the CV followed the features of polycrystalline Pt except the peak at 0.28 V in the first scan, indicating that there was an irreversible reduction/deposition in the first scan occurring on the Au(111) surface. Due to the Pt submonolayer coverage, the H UPD started later than the polycrystalline Pt, at around 0.05 V while the Pt−OH formation at 0.5 V. The H UPD charge of 78 μC/cm^2 corresponded to the Pt electrochemically active surface area (ECSA) of 0.37 ML. H UPD charge was calculated by integrating the region from −0.2 to +0.15 V with a baseline equal to the double layer current. This might be somewhat smaller than the actual physical area of deposited Pt due to the fact that Pt clusters periphery might not be active for H UPD since there is no 3-fold adsorption sites at the Pt-nanocluster perimeter. As the scan continued, j in the H UPD region decreased gradually, indicating a surface morphology change as a result of the potential sweep. ECSA was calculated based on the first scan. It is important to point out that a prominent cathode peak around 0.28 V was observed only in the first scan and was not recoverable in the following scans. In the XPS measurement we did not find the Cl^- on the surface after the first scan.

In our previous EXAFS studies,[27] we found $[PtCl_4]^{2-}$ was the main species after the SLRR reaction. The charge of this reduction peak was 93 μC/cm^2. These facts suggest that the peak observed at 0.28 V represents the following reduction reaction eq 3:

$$[PtCl_4]^{2-} + 2e^- \rightarrow Pt + 4Cl^-(aq) \quad (3)$$

Therefore, the original amount of Pt present on the Au surface might be 0.2 ML which was much smaller than 0.37 ML estimated from ECSA in the first scan. This result will be discussed later.

Ex Situ STM and XPS Results. To confirm the surface morphology of Pt/Au(111) and surface amount of Pt species after the SLRR reaction, an ex situ STM study was conducted. The imaged surface was taken from the glovebox after displacement reaction and without any further treatment to avoid possible morphology change. Figure 2 shows similar morphology with literature.[10] The upper right corner (Figure 2b) shows an enlarged image of the blue squared region in Figure 2a, with a cross section plot (Figure 2c) which showed monolayer height clusters. Analysis of 20 images gave 40 ± 6% coverage of clusters, which agreed with previous studies.[10] This STM observed coverage agreed well also with the ECSA result. Figure 2c shows the cross section of representative thin layer species with the diameter about 5 nm which was an assembly composed of 2−3 smaller clusters with about 2 nm diameter by STM.

Figure 3 shows the XPS spectrum of the Pt/Au(111) in Pt 4f region. Two species of Pt could be fitted, both with doublet energy separation of 3.4 eV and together with Au $5p_{1/2}$ peak appearing at 74.0 ± 0.3 eV.[36] The area ratio of Pt $4f_{7/2}$ and $4f_{5/2}$ was fixed at 4:3. The first Pt species had binding energy (BE) at 71.1 ± 0.3 eV, which could be assigned to the Pt^0 metal state, while the other Pt species had its BE at 72.2 ± 0.3 eV, which was clearly higher than that of the Pt metal and close to that of PtO at 72.4 eV and K_2PtCl_4 at 72.9 eV.[36] Even though the BE of the second Pt species was closer to that of

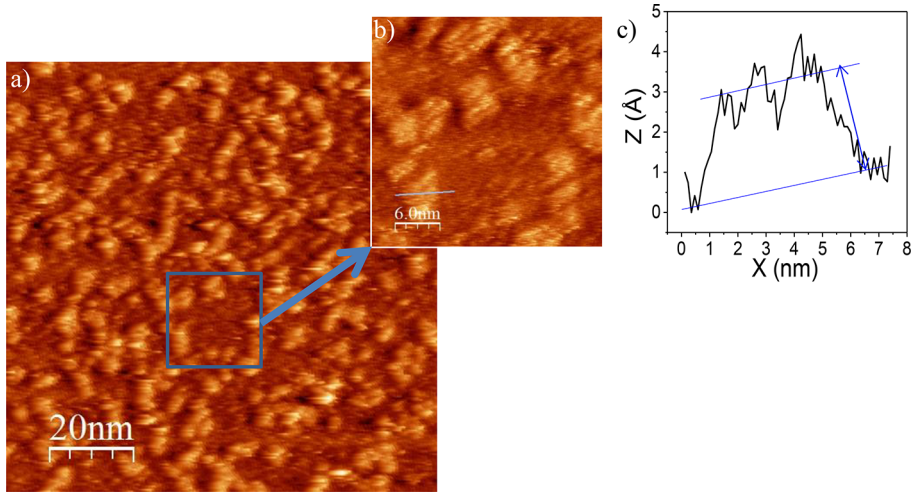

Figure 2. (a) Ex situ images of the Pt/Au(111) morphology. (b) The enlarged image of the blue squared region. (c) The height of the cluster along the line in panel b.

DOI: 10.1021/acs.jpcc.8b02218
J. Phys. Chem. C 2018, 122, 16664−16673

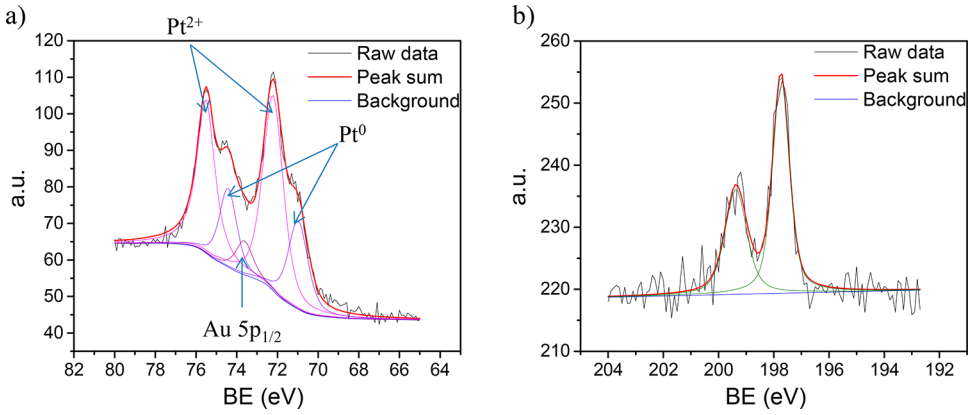

Figure 3. Narrow scan XPS of Pt/Au(111) for (a) Pt 4f and (b) Cl 2p regions.

PtO, the XPS also detected the existence of Cl (Figure 3b), which provided the possibility that there was Pt−Cl complex as a product of the SLRR reaction. Sample was protected in N_2 during the transfer from the glovebox to XPS to minimize the exposure time in air. The quantitative analysis showed that total Pt coverage was 0.34 ± 0.04 ML, which agreed with the ECSA results within the error bar. This, together with the STM image, is strong evidence that the deposited Pt was in monolayer structure and the Pt coverage was about 0.37 ± 0.05 ML. In the total 0.34 ± 0.04 ML of Pt measured by XPS, the 72.2 ± 0.3 eV (Pt^{2+}) counted for 0.22 ± 0.03 ML (64.7% in total Pt) while the 71.1 ± 0.3 eV species (Pt^0) counted for 0.12 ± 0.01 ML (35.3% in total Pt). The Cl coverage was 0.49 ± 0.01 ML, giving the ratio of Pt^{2+} and Cl of nearly 1:2, which provided the stiochiometry information on the Pt−Cl complex.

Revisit of in Situ PTRF-XAFS Results. We again discuss the XAFS results here in detail. Figure 4 shows the normalized

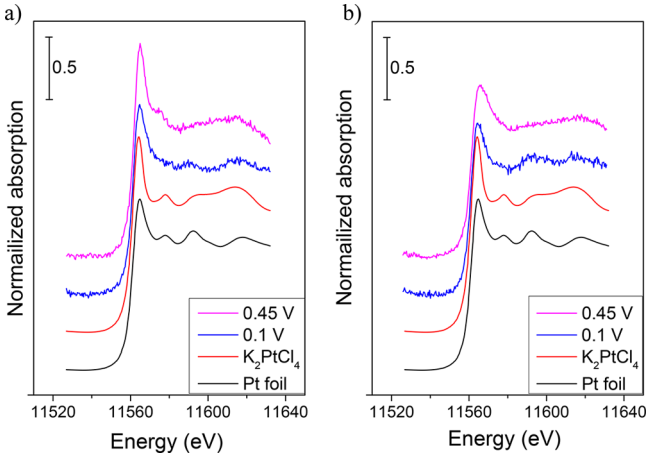

Figure 4. In situ XANES of Pt/Au(111) at 0.45 and 0.1 V, with comparison of K_2PtCl_4 and Pt foil. (a) s-polarization and (b) p-polarization.

s- and p-polarization L_3 edge XANES of the Pt monolayer measured at 0.45 and 0.1 V with comparison to the reference samples. The two potentials were chosen according to the CV shown in Figure 1 in the CV section. 0.45 V was close to the OCP and before the onset of the 0.28 V cathodic peak, while 0.1 V was after the cathodic peak and before the onset of the hydrogen adsorption. In Figure 4 the strong peak appeared around 11565 eV which was assigned to the dipole transition from $2p_{3/2}$ state to 5d empty state. The peak was called as white line (WL). The WL intensity directly reflected the amount of unfilled d states.[38]

For s-polarization Figure 4a showed the highest WL intensity at 0.45 V, while at 0.1 V WL decreased and was weaker than that of K_2PtCl_4 reference but still higher than that of the foil. The 0.45 V spectrum resembled that of K_2PtCl_4 while the spectrum of 0.1 V was similar to that of Pt foil by comparing the XANES of the K_2PtCl_4 which showed the different feature between 11590 and 11615 eV from that of foil. On the other hand, for p-polarization, WL intensities of 0.45 V was broader and slightly higher than that measured at 0.1 V, while 0.1 V was comparable with that of Pt foil. The structures above 11 590 eV showed that at the 0.45 and 0.1 V XAFS resembled that of K_2PtCl_4 and that of Pt foil, respectively, similarly to the s-polarization XANES. Both polarizations showed a lower WL intensity after sweeping the potential to 0.1 V, meaning that there was reduction of Pt species, which were associated with the cathodic peak at 0.28 V.

Figure 5a,b shows the EXAFS spectra of s- and p-polarization at 0.45 V. We proposed a $[PtCl_4]$ model in the previous EXAFS analysis[27] where the $[PtCl_4]$ molecular plane was parallel to the surface. We found that the Cl was coordinated to Pt at 0.226 nm. We did not find the Pt−O bond in the EXAFS analysis which could be clearly distinguished from Pt−Cl because phase shifts of Pt−Cl and Pt−O were π rad different from each other. According to the electrochemical results and XPS, we modified the model structure as follows. $[PtCl_4]$ was the main species, but the Pt monolayer was present as the minor species. Actually, we had the better fitting results in the mixture model of $PtCl_4$ and Pt^0. Figure 5d showed the model we used for FEFF calculation of Pt metal. Pt atom was fully coordinated in the monolayer fashion or its Pt−Pt coordination number was 6 (atom A in Figure 5d). Pt−Au distance was 0.282 nm, which was the average of bulk Pt−Pt and Au−Au distance. Pt−Pt distance was assumed to be 0.288 nm equal to the Au−Au substrate. The R factors of mixed models with different $[PtCl_4]$ compositions of both s- and p-polarizations were calculated. To generalize two polarizations, we defined the average R factor, based on the previous R factor definition in eq 2

$$R_{avg}^{\ 2} = \frac{R_s^{\ 2}/\varepsilon_s^{\ 2} + R_p^{\ 2}/\varepsilon_p^{\ 2}}{1/\varepsilon_s^{\ 2} + 1/\varepsilon_p^{\ 2}} \quad (4)$$

DOI: 10.1021/acs.jpcc.8b02218
J. Phys. Chem. C 2018, 122, 16664−16673

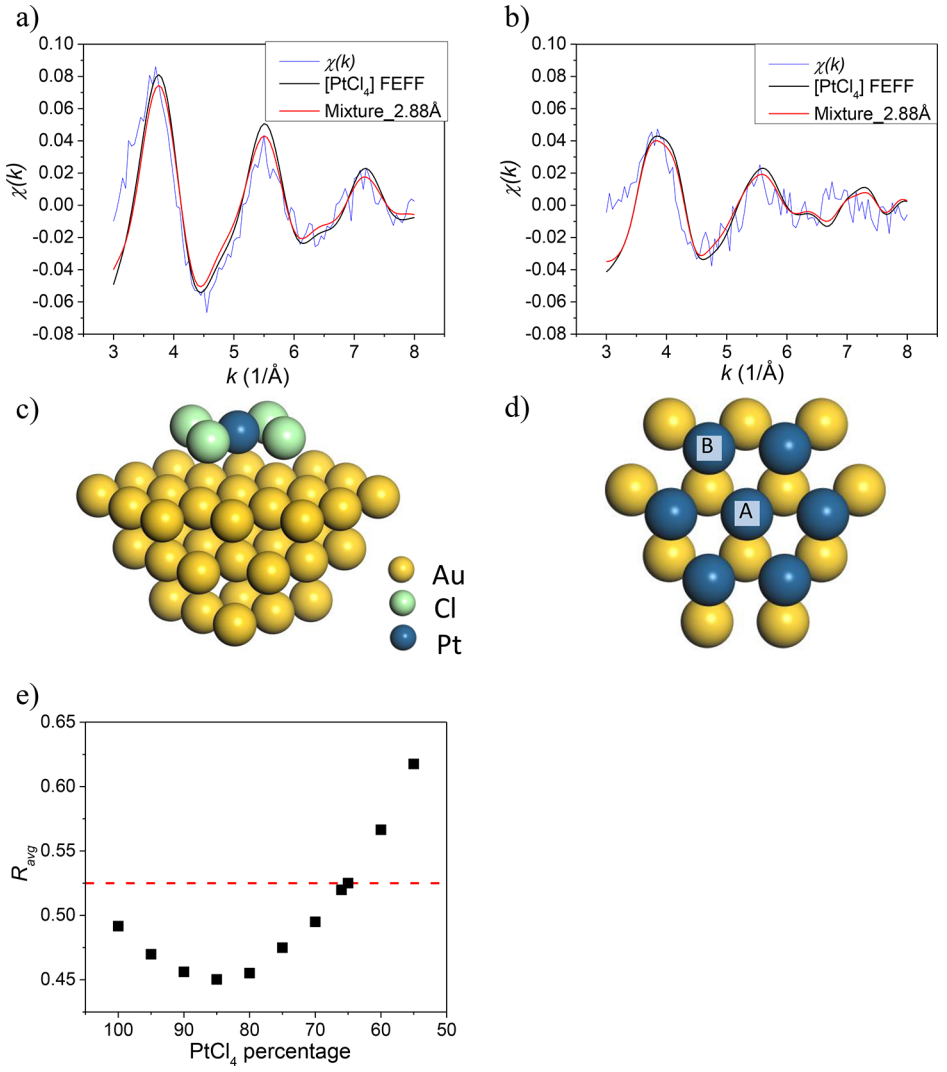

Figure 5. EXAFS comparison between experimental data at E = 0.45 V and FEFF calculation for the $[PtCl_4]$ model and the following mixture model. (a) s-polarization, (b) p-polarization, (c) $[PtCl_4]$ model structure, (d) Pt metal cluster model, and (e) Hamilton test for the average R factor (eq 4), with the acceptable value (R_{avg} = 0.52 red dotted line) when significant level was 0.05. Pt−Pt bond distance was 2.88 Å. Coordination number of Pt with in-plane Pt was 6.

where ε_s^2 and ε_p^2 are the averaged standard deviation for both s- and p-polarization. R_{avg}^2 of mixed spectra were calculated with x ($0 < x < 1$, tep 0.05) $[PtCl_4]$ and $(1 - x)$ Pt metal monolayer.

Figure 5e showed the R_{avg} change as a function of $[PtCl_4]$ amount. The minimum R_{avg} = 0.45 was achieved when x = 0.85 for bond distances at 0.288 nm while R_{avg} with no Pt metal was 0.50. The acceptable range of x was calculated using F-test. The degree of freedom for R_{avg} was 16. The confidence interval when significance level α was set to 0.05 was $x \in [1, 0.66]$ (Figure 5e). The mixed FEFF spectra with Pt complex composition of 0.85 are plotted as the red curve in Figure 5a,b. To optimize the Pt−Pt bond distance, we tested several models by varying the Pt−Pt bond distance. The two cases with different distances (i.e., 0.288 and 0.277 nm) were tested, which corresponded to the Au(111) substrate lattice constant and the Pt bulk, respectively, and the 0.288 nm gave better fitting. Note that we assumed the Pt one monolayer with an infinite size. However, the STM results indicated that cluster size was 4−6 nm in diameter, indicating the fraction of $[PtCl_4]$ might be less than 0.85 and will be discussed in the following section.

Oxidation State of Pt in $[PtCl_4]$. Based on XPS analysis, two chemical states of Pt were observed, Pt^{2+} and Pt^0. EXAFS analysis indicated no contradiction if both species were present. Electrochemical results showed that the charge corresponding to the 0.28 V cathodic peak in the first scan was 93 $\mu C/cm^2$, while the H UPD charge was 78 $\mu C/cm^2$. Without considering other characterization results, knowing that the $[PtCl_6]^{2-}$ as the starting compound and following reduction paths

$$Pt^{n+} + ne^- \rightarrow Pt \quad (5)$$

The percentage of Pt^{n+} on Au surface would be 119%, 60%, 40% and 30%, when n was 1, 2, 3, and 4, respectively. Based on the XAFS simulation which showed $[PtCl_4]$ might be between 0.66 and 1.0, although n = 2 does not fall in this region, we have to remember that Pt metal oscillation used previously did not consider the actual Pt cluster size, which will eventually decrease the complex percentage. Therefore, it is reasonable to propose n = 2 at this point. Consequently, the most plausible

DOI: 10.1021/acs.jpcc.8b02218
J. Phys. Chem. C 2018, 122, 16664−16673

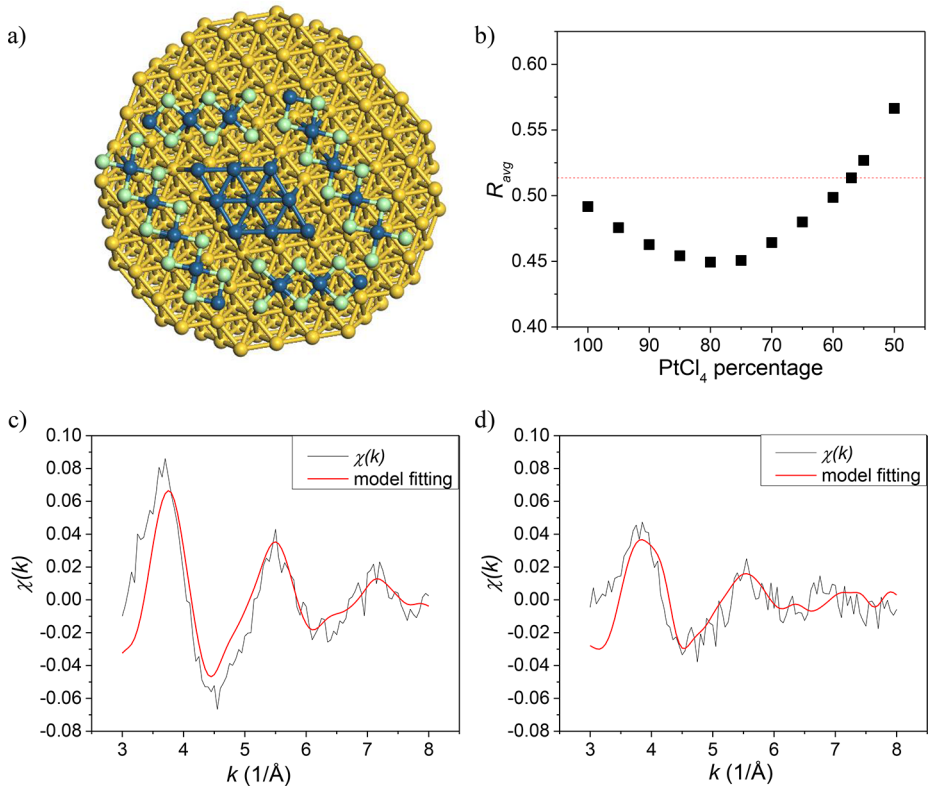

Figure 6. (a) Proposed metal (40%) + complex (60%) model on Au(111), with complex adsorbed on the edge of metal clusters. Green, Cl; blue, Pt; yellow, Au. (b) Recalculated R_{avg} based on the size of Pt cluster in this model. (c) s-polarization of the model fitting results, in comparison with experimental data. (d) p-polarization.

species was the $[PtCl_4]^{2-}$ complex, which agreed with XPS and XAFS results. Since we could only observe the homogeneous Pt clusters by STM, $[PtCl_4]^{2-}$ might be adsorbed around the nucleated Pt clusters (Figure 6a). The surrounding $[PtCl_4]^{2-}$ has a similar local structure to $PtCl_2$ where two Pt shared two Cl and one Pt was surrounded by four Cl to form square structure. Although details of the structure were discussed later the $[PtCl_4]^{2-}$ found here was denoted as $[PtCl_2$-square$]$ hereinafter.

Based on the model structure that one monolayer metal core (40%) + $[PtCl_2$-square$]$ shell (60%) with 2.2 nm cluster shown in Figure 6a), R_{avg} dependence of Pt complex percentage was recalculated, and the corresponding acceptable range was $x \in [1, 0.57]$ with the same significant level. Now $n = 2$ fell into the Pt complex region by EXAFS modeling. We calculated the EXAFS spectra of this model, with the assumption of Pt−Pt bond distance to be 0.288 nm and the size of $[PtCl_4]$ unit in $[PtCl_2$-square$]$ to be 0.82 nm. The model gave $R_{avg} = 0.45$, and the spectra (Figure 6c,d) were plausible even compared to the best fitting results. In this model, Cl was shared by two adjacent $[PtCl_4]$ units based on the 2:1 ratio of Cl to Pt from the XPS result. Following the above analysis by assuming the 60% $[PtCl_2$-square$]$ and 40% metallic state, the s- and p-polarization XANES we measured should also contain both contributions from $[PtCl_2$-square$]$ and Pt−Pt bond. The 0.1 V XANES spectra in Figure 4 were used here to represent the metallic Pt monolayer clusters on Au(111) on the assumption that the whole Pt L_3 edge XANES should have similar spectral features inside the whole cluster. Consequently, the measured XANES at 0.45 V for both polarizations could be expressed as

$$\mu_{0.45V} = 0.6\mu_{[PtCl_2-square]} + 0.4\mu_{0.1V} \quad (6)$$

Assuming the Pt local structure in $[PtCl_2$-square$]$ and its random orientation shown in Figure 5c), the unpolarized spectrum of $[PtCl_2$-square$]$, μ_{unpol}, could be calculated by the following equation:

$$\mu_{unpol} = \frac{2\mu_s + \mu_p}{3} \quad (7)$$

where μ_s and μ_p stands for the $\mu_{[PtCl2-square]}$ in s- and p-polarization, respectively.

Figure 7 shows the integrated unpolarized spectrum based on the eq 6 and 7 together with the experimental value. The

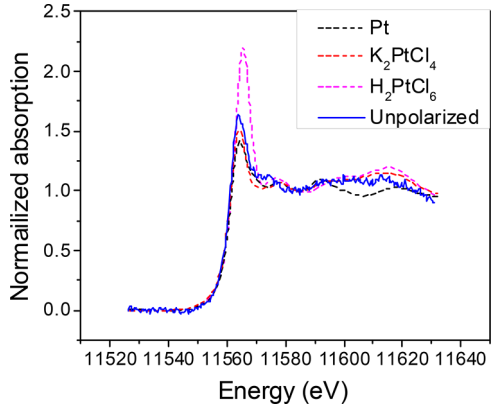

Figure 7. Calculated $[PtCl_2$-square$]$ XANES (unpolarized) according to eqs 6 and 7 with other reference spectra.

DOI: 10.1021/acs.jpcc.8b02218
J. Phys. Chem. C 2018, 122, 16664−16673

unpolarized spectrum was best expressed by the reference $[PtCl_4]^{2-}$ data both in WL intensity and region above 11 590 eV, which resembled Pt−Cl oscillation. The difference may come from the different local structures in $[PtCl_4]^{2-}$ and Pt−Au interaction. Therefore, one possible model would be $[PtCl_2$-square$]$ around the nucleated Pt clusters.

Comparison with $PtCl_2$ and $PtCl_2$-Square. The $PtCl_2$ bulk crystal[39] and the $[PtCl_2$-square$]$ found here have both a square planar $[PtCl_4]$ unit around Pt(2+). Each unit is linked with each other by sharing two chlorides. The difference is the dimensionality. In the $PtCl_2$ crystal, 6 $PtCl_4$ units get together to form the $PtCl_2$ cubic structure, denoted as Pt_6Cl_{12} where each face is composed of a $PtCl_4$ unit. In the $[PtCl_2$-square$]$, all $PtCl_4$ units are in the same plain. Although the structure satisfies the observed data, yet one may ask why no Pt−Pt distance is observed in EXAFS. We do not know the exact answer, but the structure has some disorder in Pt−Pt to form the ring around the Pt nucleus. The reason why the 3-dimensional $[PtCl_4]$ unit like $PtCl_2$ is not formed on the Au may be the Au−$[PtCl_4]$ interaction in $[PtCl_2$-square$]$ structure to form all $PtCl_4$ parallel to the Au surface.

Reaction Stoichiometry. Assuming the oxidation state of Pt as 2+ for $[PtCl_2$-square$]$, we discussed the reaction stoichiometry during the displacement reactions based on the electrochemical, XAFS, XPS, and AFM results. From the analysis above, we had proposed that the surface species of Pt was a mixture of $[PtCl_2$-square$]$ and metallic Pt monolayer cluster ($Pt_{9\pm2}$) with 3:2. From the CV of Pt/Au(111) in 0.1 M $HClO_4$, the charge associated with the cathodic peak in the first scan was 93 $\mu C/cm^2$, which could be assigned to the reduction of $[PtCl_2$-square$]$, where Pt^{2+} was reduced and two-electron charge transfer was involved. There are two possibilities for the origin of the $[PtCl_2$-square$]$, from displacement of Cu UPD by partially reducing the $[PtCl_6]^{2-}$ (eq 8) and from the spontaneous deposition of Pt on Au surface[40] (eq 9). We discuss the two scenarios along with the oxidation state of Cu after displacement reaction.

$$\begin{cases} [PtCl_6]^{2-} + 2e^- \rightarrow [PtCl_2 - \text{square}] + 4Cl^- & 60\% \\ [PtCl_6]^{2-} + 4e^- \rightarrow Pt + 6Cl^- & 40\% \end{cases} \quad (8)$$

$$\begin{cases} \text{spontaneous deposition} & 60\% \\ [PtCl_6]^{2-} + 4e^- \rightarrow Pt + 6Cl^- & 40\% \end{cases} \quad (9)$$

Assuming that the $[PtCl_2$-square$]$ was reduced on the surface as a product of the displacement reaction of Cu (eq 8), in order to reduce the original $[PtCl_6]^{2-}$, the same amount of charge as required for $[PtCl_2$-square$]$ reduction to Pt, i.e., 93 $\mu C/cm^2$, was necessary. Meanwhile, to deposit the other 40% of metallic Pt species, $[PtCl_6]^{2-}$ was reduced to Pt^0, which required 125 $\mu C/cm^2$ charge (four-electron transfer). It gave the total charge of 218 (= 125 + 93) $\mu C/cm^2$. In the scenario of eq 9, if the origin of $[PtCl_2$-square$]$ reduction comes from spontaneous deposition of $PtCl_6^{2-}$ on Au as assumed in ref 40, only 125 $\mu C/cm^2$ charge was necessary to reduce $[PtCl_6]^{2-}$ to Pt^0.

For the Cu UPD, we checked the Cu amount by XPS which was 0.62 ML corresponding to the charge of 273 $\mu C/cm^2$, if the Cu UPD layer was oxidized into Cu^{2+} (eq 10). There was also possibilities for the Cu oxidation state, which was suggested by the previous study that due to the excessive amount of Cl^-, Cu(I), instead of Cu(II), was more stable in aqueous solutions[10] (eq 11). Following this assumption, oxidation of Cu would be accompanied by providing electron of 136.5(=273/2) $\mu C/cm^2$.

$$Cu \rightarrow Cu^{2+} + 2e^- \quad (10)$$

$$Cu + 2Cl^- \rightarrow [CuCl_2]^- + e^- \quad (11)$$

Since the amount of the Cu was too small ($\sim 10^{-3}$ ppm), it was difficult to identify the Cu species in solution directly. We thought the following four scenarios. To make a clear comparison, the calculated charges with different Cu oxidation state and surface $[PtCl_2$-square$]$ origin are listed in Table 1.

Table 1. Charge Comparison for Different Pt Origins and Cu Oxidations States

entry	scenario	charge for reduction of Pt ($\mu C/cm^2$)	charge from oxidation of Cu ($\mu C/cm^2$)
I	Cu(I) (eq 11), Pt spon. (eq 9)	125	136.5
II	Cu(II) (eq 10), Pt disp. (eq 8)	218	273
III	Cu(II) (eq 10), Pt spon. (eq 9)	125	273
IV	Cu(I) (eq 11), Pt disp. (eq 8)	218	136.5

Cu(I) means that eq 11 occurred, and the product was $[CuCl_2]^-$ while Cu(II) means the Cu^{2+} was created. Pt spon. represents that surface Pt(2+) was created after the spontaneous reaction, while Pt disp. means that surface Pt(2+) was deposited by the galvanic displacement reaction.

It is evident that the combination of Cu(I) and Pt spontaneous deposition presented smallest error (scenario I), i.e., the same stoichiometry proposed in ref 10. The overall reaction follows:

$$[PtCl_6]^{2-} + 4Cu^0 + 2Cl^- \rightarrow Pt^0 + 4[CuCl_2]^- \quad (12)$$

Note that this mechanism requires extra Cl^- supply. The formation of Cu^+ is promoted by the existence of Cl^- in the solution. The origin of the extra Cl^- supply may come from the spontaneous deposition of $[PtCl_6]^{2-}$. As we mentioned in the Experimental Section we could not obtain the Pt monolayer by SLRR using $[PtCl_4]^{2-}$. This might be related to the fewer Cl^- available in the reaction of $[PtCl_4]^{2-}$. To verify this mechanism, we measured the Pt coverage change as a function of Cu UPD coverage. A similar measurement was conducted in ref 10, but the coverage of Pt was determined using XPS in our study. Results are shown in Figure 8. One point with about 0.1 ML coverage to avoid the extreme situation of bare Au where spontaneous deposition happens. The slope obtained from linear fitting of the three data points was 0.23 ± 0.04. It means one Pt atom was exchanged with about 4 Cu, agreed well with eq 12. The highest Pt coverage could be obtained with the displacement reaction was about 0.34 ML by XPS, and about 0.2 ML coverage could be extrapolated when $\theta_{Cu} = 0$. The portion of Pt from spontaneous deposition should be in 2+ without any further treatment. The ratio of 0.2 ML (59%) Pt(2+) vs 0.14 ML (41%) for Pt(0) agrees well with the electrochemical, XPS and EXAFS results (3:2). The spontaneous deposition might occur by the reaction of surface Au and $[PtCl_6]^{2-}$ to give Pt (II) chloride complex. Here we used the term, Pt(II) chloride complex, because we did not

DOI: 10.1021/acs.jpcc.8b02218
J. Phys. Chem. C 2018, 122, 16664−16673

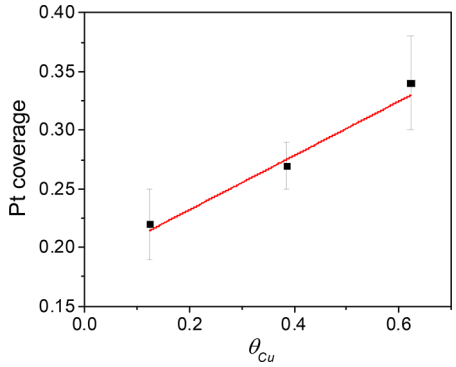

Figure 8. Pt coverage change as a function of Cu UPD coverage. Slope = 0.23 ± 0.04.

explicitly characterize Pt(II) chloride complex structure as a product of the spontaneous reaction. However, we could say the Pt(II) chloride species should have strong interaction with Au surface similar to [$PtCl_2$-square].

To confirm the interaction of Pt(II) chloride species with Au substrate was strong, we carried out the following experiment. The displacement reaction was repeated five times to achieve more Pt deposition (Pt/Au(111)_5). Figure 9 was the STM image of the Pt/Au(111)_5 surface after five cycles and the linear sweep voltammetry (LSV) of the reduction of the Pt complex of Pt/Au(111)_1 and Pt/Au(111)_5. STM showed an almost fully covered surface with more densely clusters which had similar size but two-atomic-layer height comparing to the surface after 1 deposition cycle. The cathodic LSV scan indicated a smaller reduction peak for the Pt/Au(111)_5 than that of the Pt/Au(111)_1 surface. This could be well explained by the fact that less exposed Au means weaker interaction with Pt complexes, which agreed with the literature.[7,25]

CONCLUSION

Surface structure of Pt/Au(111) deposited by SLRR of Cu UPD was revealed by XAFS, XPS, STM, together with electrochemical methods. We proposed that a new model including adsorption of [$PtCl_2$-square] where [$PtCl_4$] unit was arranged parallel to the Au. This pathway to form [$PtCl_2$-square] counted for 60% of the total amount of deposited Pt, while the remaining (40%) was Pt metal obtained by SLRR. This model is consistent with all of the CV, XAFS, and XPS results. The model is different from what was expected for the Pt structures after SLRR reactions[13] and what we proposed in the previous paper.[27] Based on this model, reaction mechanism was proposed and proved to be consistent with the previous STM study.[10] The stabilization of Cu^+ in the existence of Cl^- might be the reason for the low efficiency of SLRR using $[PtCl_4]^{2-}$ and Cu as sacrificial metal in $HClO_4$ environment. The [$PtCl_2$-square] was a product of spontaneous deposition and was found to have strong interaction with the bare Au surface which could be related to the reaction kinetics change as the deposited Pt amount increased.[25]

ASSOCIATED CONTENT

Supporting Information

The Supporting Information is available free of charge on the ACS Publications website at DOI: 10.1021/acs.jpcc.8b02218.

CV of Au(111) and Cu UPD and XPS measurement of Cu on Au (111) after the Cu UPD (PDF)

AUTHOR INFORMATION

Corresponding Author

*E-mail: askr@cat.hokudai.ac.jp.

ORCID

Takahiro Wada: 0000-0001-8456-8282

Kiyotaka Asakura: 0000-0003-1077-5996

Notes

The authors declare no competing financial interest.

ACKNOWLEDGMENTS

The authors would like to acknowledge NEDO PEFCs project for their financial support. S.R.B. acknowledges support from NSF-CBET No. 1605331 program. The work was carried out under the approval of PAC (Proposal No. 2015G070 and 2016G035) and the proposal number of SPring 8 (2016B7904). We also would like to thank Dr. Y. Niwa, Dr. H. Nitani, Dr. H. Abe, and Prof. M. Kimura in PF, KEK and Dr. O. Sekizawa and T. Uruga in SPring−8, and Prof. Y. Iwasawa in ECU for their technical support and discussion. The in situ XAFS cell and electrochemical cells were made by Technical Division of Institute for Catalysis, Hokkaido University.

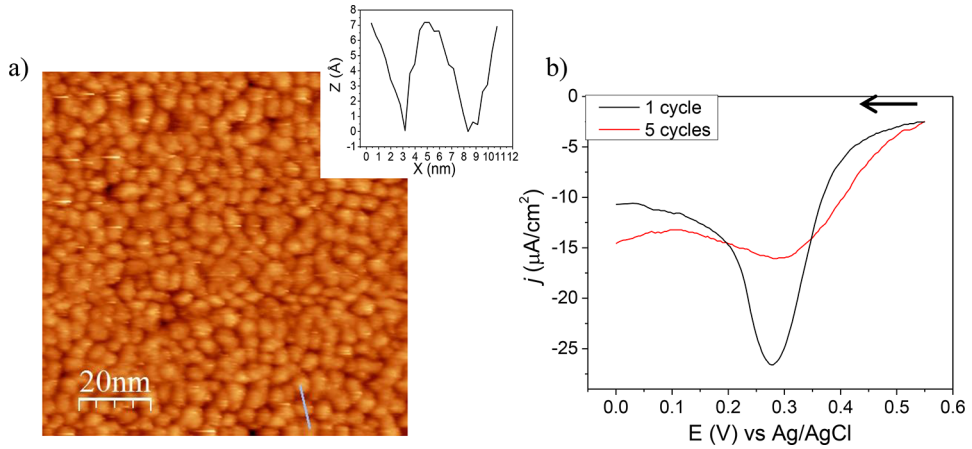

Figure 9. (a) STM image of Pt/Au(111)_5 surface with cross section shown in upper left corner. (b) LSV of Pt/Au(111)_1 and Pt/Au(111)_5 in 0.1 M $HClO_4$. Arrow indicates the scan direction. Scan rate: 0.05 V/s.

DOI: 10.1021/acs.jpcc.8b02218
J. Phys. Chem. C 2018, 122, 16664−16673

REFERENCES

(1) Yu, W. T.; Porosoff, M. D.; Chen, J. G. G. Review of Pt-Based Bimetallic Catalysis: From Model Surfaces to Supported Catalysts. *Chem. Rev.* **2012**, *112*, 5780−5817.

(2) Johnson, R. W.; Hultqvist, A.; Bent, S. F. A Brief Review of Atomic Layer Deposition: From Fundamentals to Applications. Mater. *Mater. Today* **2014**, *17*, 236−246.

(3) Lairson, B.; Visokay, M.; Sinclair, R.; Hagstrom, S.; Clemens, B. Epitaxial Pt (001), Pt (110), and Pt (111) Films on MgO (001), MgO (110), MgO (111), and Al_2O_3 (0001). *Appl. Phys. Lett.* **1992**, *61*, 1390−1392.

(4) Reina, A.; Jia, X.; Ho, J.; Nezich, D.; Son, H.; Bulovic, V.; Dresselhaus, M. S.; Kong, J. Large Area, Few-Layer Graphene Films on Arbitrary Substrates by Chemical Vapor Deposition. *Nano Lett.* **2009**, *9*, 30−35.

(5) Selvakumar, N.; Barshilia, H. C. Review of Physical Vapor Deposited (PVD) Spectrally Selective Coatings for Mid-and High-Temperature Solar Thermal Applications. Solar Energy Mater. *Sol. Energy Mater. Sol. Cells* **2012**, *98*, 1−23.

(6) Gregory, B. W.; Stickney, J. L. Electrochemical Atomic Layer Epitaxy (ECALE). *J. Electroanal. Chem. Interfacial Electrochem.* **1991**, *300*, 543−561.

(7) Waibel, H. F.; Kleinert, M.; Kibler, L. A.; Kolb, D. M. Initial Stages of Pt Deposition on Au(111) and Au(100). *Electrochim. Acta* **2002**, *47*, 1461−1467.

(8) Brankovic, S. R.; Wang, J. X.; Adzic, R. R. Metal Monolayer Deposition by Replacement of Metal Adlayers on Electrode Surfaces. *Surf. Sci.* **2001**, *474*, L173−L179.

(9) Debe, M. K. Electrocatalyst Approaches and Challenges for Automotive Fuel Cells. *Nature* **2012**, *486*, 43−51.

(10) Gokcen, D.; Bae, S. E.; Brankovic, S. R. Stoichiometry of Pt Submonolayer Deposition Via Surface-Limited Redox Replacement Reaction. *J. Electrochem. Soc.* **2010**, *157*, D582−D587.

(11) Gokcen, D.; Bae, S. E.; Brankovic, S. R. Reaction Kinetics of Metal Deposition Via Surface Limited Red-Ox Replacement of Underpotentially Deposited Metal Monolayers. Electrochim. *Electrochim. Acta* **2011**, *56*, 5545−5553.

(12) Vasilic, R.; Viyannalage, L. T.; Dimitrov, N. Epitaxial Growth of Ag on Au(111) by Galvanic Displacement of Pb and Tl Monolayers. *J. Electrochem. Soc.* **2006**, *153*, C648−C655.

(13) Gokcen, D.; Yuan, Q. Y.; Brankovic, S. R. Nucleation of Pt Monolayers Deposited Via Surface Limited Redox Replacement Reaction. *J. Electrochem. Soc.* **2014**, *161*, D3051−D3056.

(14) Fayette, M.; Liu, Y.; Bertrand, D.; Nutariya, J.; Vasiljevic, N.; Dimitrov, N. From Au to Pt Via Surface Limited Redox Replacement of Pb UPD in One-Cell Configuration. *Langmuir* **2011**, *27*, 5650−5658.

(15) Jayaraju, N.; Vairavapandian, D.; Kim, Y. G.; Banga, D.; Stickney, J. L. Electrochemical Atomic Layer Deposition (E-ALD) of Pt Nanofilms Using SLRR Cycles. *J. Electrochem. Soc.* **2012**, *159*, D616−D622.

(16) Zhang, J. L.; Vukmirovic, M. B.; Sasaki, K.; Nilekar, A. U.; Mavrikakis, M.; Adzic, R. R. Mixed-Metal Pt Monolayer Electrocatalysts for Enhanced Oxygen Reduction Kinetics. *J. Am. Chem. Soc.* **2005**, *127*, 12480−12481.

(17) Vukmirovic, M. B.; Zhang, J.; Sasaki, K.; Nilekar, A. U.; Uribe, F.; Mavrikakis, M.; Adzic, R. R. Platinum Monolayer Electrocatalysts for Oxygen Reduction. *Electrochim. Acta* **2007**, *52*, 2257−2263.

(18) Mrozek, M. F.; Xie, Y.; Weaver, M. J. Surface-Enhanced Raman Scattering on Uniform Platinum-Group Overlayers: Preparation by Redox Replacement of Underpotential-Deposited Metals on Gold. *Anal. Chem.* **2001**, *73*, 5953−5960.

(19) Sheridan, L. B.; Kim, Y. G.; Perdue, B. R.; Jagannathan, K.; Stickney, J. L.; Robinson, D. B. Hydrogen Adsorption, Absorption, and Desorption at Palladium Nanofilms Formed on Au(111) by Electrochemical Atomic Layer Deposition (E-ALD): Studies Using Voltammetry and in Situ Scanning Tunneling Microscopy. *J. Phys. Chem. C* **2013**, *117*, 15728−15740.

(20) Zhang, J.; Sasaki, K.; Sutter, E.; Adzic, R. R. Stabilization of Platinum Oxygen-Reduction Electrocatalysts Using Gold Clusters. *Science* **2007**, *315*, 220−222.

(21) Thambidurai, C.; Kim, Y. G.; Stickney, J. L. Electrodeposition of Ru by Atomic Layer Deposition (ALD). *Electrochim. Acta* **2008**, *53*, 6157−6164.

(22) Thambidurai, C.; Kim, Y.-G.; Jayaraju, N.; Venkatasamy, V.; Stickney, J. Copper Nanofilm Formation by Electrochemical Ald. *J. Electrochem. Soc.* **2009**, *156*, D261−D268.

(23) Venkatraman, K.; Dordi, Y.; Akolkar, R. Electrochemical Atomic Layer Deposition of Cobalt Enabled by the Surface-Limited Redox Replacement of Underpotentially Deposited Zinc. *J. Electrochem. Soc.* **2017**, *164*, D104−D109.

(24) Dimitrov, N. Recent Advances in the Growth of Metals, Alloys, and Multilayers by Surface Limited Redox Replacement (SLRR) Based Approaches. *Electrochim. Acta* **2016**, *209*, 599−622.

(25) Mkwizu, T. S.; Cukrowski, I. Physico-Chemical Modelling of Adlayer Phase Formation Via Surface-Limited Reactions of Copper in Relation to Sequential Electrodeposition of Multilayered Platinum on Crystalline Gold. Electrochim. *Electrochim. Acta* **2014**, *147*, 432−441.

(26) Bulut, E.; Wu, D. J.; Dole, N.; Kilic, H.; Brankovic, S. R. Reaction Kinetics of Metal Deposition Via Surface Limited Redox Replacement of Underpotentially Deposited Monolayer Studied by Surface Reflectivity and Open Circuit Potential Measurements. *J. Electrochem. Soc.* **2017**, *164*, D159−D168.

(27) Yuan, Q. Y.; Takakusagi, S.; Wakisaka, Y.; Uemura, H.; Wada, T.; Ariga, H.; Asakura, K. Polarization-Dependent Total Reflection Fluorescence X-Ray Absorption Fine Structure (Ptrf-XAFS) Studies on the Structure of a Pt Monolayer on Au (111) Prepared by the Surface-Limited Redox Replacement Reaction. *Chem. Lett.* **2017**, *46*, 1250−1253.

(28) Takakusagi, S.; Chun, W. J.; Uehara, H.; Asakura, K.; Iwasawa, Y. Polarization-Dependent Total-Reflection Fluorescence X-Ray Absorption Fine Structure for 3d Structural Determination and Surface Fine Tuning. *Top. Catal.* **2013**, *56*, 1477−1487.

(29) Uehara, H.; Bin Hanaffi, M. H.; Koike, Y.; Fujikawa, K.; Suzuki, S.; Ariga, H.; Takakusagi, S.; Chun, W. J.; Iwasawa, Y.; Asakura, K. Anisotropic Growth of a Nickel Trimer Formed on a Highly-Stepped TiO_2(110) Surface. *Chem. Phys. Lett.* **2013**, *570*, 64−69.

(30) Uehara, H.; Uemura, Y.; Ogawa, T.; Kono, K.; Ueno, R.; Niwa, Y.; Nitani, H.; Abe, H.; Takakusagi, S.; Nomura, M.; et al. Situ Back-Side Illumination Fluorescence Xafs (Bi-Fxafs) Studies on Platinum Nanoparticles Deposited on a Hopg Surface as a Model Fuel Cell: A New Approach to the Pt-Hopg Electrode/Electrolyte Interface. *Phys. Chem. Chem. Phys.* **2014**, *16*, 13748−13754.

(31) Takakusagi, S.; Kunimoto, A.; Sirisit, N.; Uehara, H.; Ohba, T.; Uemuara, Y.; Wada, T.; Ariga, H.; Chun, W. J.; Iwasawa, Y.; et al. A New Indicator for Single Metal Dispersion on a Tio2(110) Surface Premodified with a Mercapto Compound. *J. Phys. Chem. C* **2016**, *120*, 15785−15791.

(32) Asakura, K. In *X-Ray Absorption Fine Structure for Catalyst and Surfaces*; Iwasawa, Y., Ed.; World Scientific: Singapore, 1996; Vol. 2, p 33.

(33) Rehr, J. J.; Albers, R. C. Theoretical Approaches to X-Ray Absorption Fine Structure. *Rev. Mod. Phys.* **2000**, *72*, 621−654.

(34) Ankudinov, A. L.; Ravel, B.; Rehr, J. J.; Conradson, S. D. Real-Space Multiple-Scattering Calculation and Interpretation of X-Ray-Absorption near-Edge Structure. *Phys. Rev. B: Condens. Matter Mater. Phys.* **1998**, *58*, 7565−7576.

(35) Heald, S. M.; Stern, E. A. Anisotropic X-Ray Absorption in Layered Compounds. *Phys. Rev. B* **1977**, *16*, 5549−5559.

(36) JOEL *Handbook of X-Ray Photoelectron Spectroscopy*; JOEL: 1991.

(37) Horcas, I.; Fernández, R.; Gomez-Rodriguez, J.; Colchero, J.; Gómez-Herrero, J.; Baro, A. Wsxm: A Software for Scanning Probe Microscopy and a Tool for Nanotechnology. *Rev. Sci. Instrum.* **2007**, *78*, 013705.

(38) Mansour, A. N.; Cook, J. W.; Sayers, D. E. Quantitative Technique for the Determination of the Number of Unoccupied D-

DOI: 10.1021/acs.jpcc.8b02218
J. Phys. Chem. C 2018, 122, 16664−16673

Electron States in a Platinum Catalyst Using the $L_{2,3}$ X-Ray Absorption-Edge Spectra. *J. Phys. Chem.* **1984**, *88*, 2330−2334.
(39) von Schnering, H. G.; Chang, J. H.; Peters, K.; Peters, E. M.; Wagner, F. R.; Grin, Y.; Thiele, G. Structure and Bonding of the Hexameric Platinum (II) Dichloride, Pt6cl12 (B-Ptcl2). *Z. Anorg. Allg. Chem.* **2003**, *629*, 516−522.
(40) Strbac, S.; Petrovic, S.; Vasilic, R.; Kovac, J.; Zalar, A.; Rakocevic, Z. Carbon Monoxide Oxidation on Au(111) Surface Decorated by Spontaneously Deposited Pt. *Electrochim. Acta* **2007**, *53*, 998−1005.

DOI: 10.1021/acs.jpcc.8b02218
J. Phys. Chem. C 2018, 122, 16664−16673